

Shot noise induced by nonequilibrium spin-dependent chemical potentials

Tomonori Arakawa,^{1,*} Junichi Shiogai,² Mariusz Ciorga,³ Martin Utz,³ Dieter Schuh,³ Makoto Kohda,^{2,4} Junsaku Nitta,² Dominique Bougeard,³ Dieter Weiss,³ Teruo Ono,⁵ and Kensuke Kobayashi^{1,†}

¹*Department of Physics, Graduate School of Science, Osaka University,
1-1 Machikaneyama, Toyonaka, Osaka 560-0043, Japan*

²*Department of Materials Science, Tohoku University, 980-8579 Sendai, Miyagi, Japan*

³*Institute of Experimental and Applied Physics, University of Regensburg, D-93040 Regensburg, Germany*

⁴*PRESTO, Japan Science and Technology Agency, 332-0012 Kawaguchi, Saitama, Japan*

⁵*Institute for Chemical Research, Kyoto University, 611-0011 Uji, Kyoto, Japan*

(Dated: February 2, 2019)

When electric current passes across a potential barrier, the partition process of electrons at the barrier gives rise to the shot noise, reflecting the discrete nature of electric charge. Here, beyond this conventional charge shot noise, we bring to light “spin” shot noise associated with spin current that is induced by nonequilibrium spin-dependent chemical potentials in an all-semiconductor lateral spin valve device. We prove that the detected spin shot noise is proportional to the spin current and the resultant Fano factor directly evidences that the spin degree of freedom is preserved in the tunneling process. This demonstrated spin shot noise can serve as a unique probe of spin noise spectroscopy to explore nonequilibrium spin transport.

In 1918, Schottky argued that the electric flow in a vacuum tube fluctuates in a unique way such that the spectral density of the fluctuations is proportional to the unit of charge $-e$ ($e > 0$) and to the mean current [1]. This is the shot noise, the direct consequence of the discreteness of the electron charge. Now, as an electron possesses not only charge but also spin, one may ask how the discreteness of electron spin affects the current fluctuations. Although such spin-dependent shot noise has been discussed theoretically in various contexts [2–9], it has never been evidenced experimentally.

Here, we report a related case, namely, the shot noise driven by nonequilibrium spin-dependent chemical potentials [9]. The current noise spectral density S_I ($\equiv \langle (\delta I)^2 \rangle / \Delta\nu$) in a conventional tunneling barrier, exactly as in the vacuum tube, is given by $S_I = 2e|\langle I \rangle|$, where $\langle I \rangle$ and $\langle (\delta I)^2 \rangle$ are the average and variance of the current, respectively. $\Delta\nu$ is the Nyquist measurement bandwidth. In the presence of spin-dependent chemical potentials, a general way to deal with the current is the two-fluid model, where the electric current consists of a current carried by spin-up electrons (I_\uparrow) and one with spin-down electrons (I_\downarrow). We can define the charge current $I_C^* \equiv I_\uparrow + I_\downarrow$ and spin current $I_S^* \equiv I_\uparrow - I_\downarrow$ [10]. For simplicity, we assume that there is no spin-flip event in the tunneling process. Correspondingly, we define a charge shot noise $S_C^* \equiv 2e|\langle I_C^* \rangle|$ and a “spin shot noise” $S_S^* \equiv 2e|\langle I_S^* \rangle|$. Note that this is more than a nominal decomposition. Suppose that $\langle I_\uparrow \rangle = -\langle I_\downarrow \rangle \neq 0$ so that $\langle I_C^* \rangle = 0$ and $\langle I_S^* \rangle \neq 0$ (pure spin current). Even without any net charge flow, the noise would be finite and given by $S_S^* = 2e(|\langle I_\uparrow \rangle| + |\langle I_\downarrow \rangle|)$. The above discussion can be easily extended to general situations with arbitrary I_C^* and I_S^* .

In this letter we demonstrate the relevance of this concept by measuring shot noise across a tunneling barrier in the presence of spin accumulation. We have successfully extracted charge and spin currents and charge and spin shot noise, and found that the resulting Fano factor directly verifies that the spin degree of freedom is preserved in the tunneling process. Moreover we have quantitatively evaluated the smearing of chemical potentials induced by non-local spin injection, which hides the observation of the spin shot noise caused by pure spin current. Given the importance of shot noise in various fields, especially in device technology [11] and mesoscopic physics [12–14], spin shot noise could not only serve as a unique probe to explore spin-dependent nonequilibrium electrons transport but also shed new light on the recently emerging field of spin noise spectroscopy [15–18].

Nonequilibrium spin-dependent chemical potentials can be generated using an electrical spin injection method [19, 20]. To this end, we prepared a lateral all semiconductor spin valve device, which was fabricated from a single epitaxial wafer grown by molecular beam epitaxy on a (001) GaAs substrate, consisting of, in the growth order, GaAs buffer, AlGaAs/GaAs superlattice, 1 μm n -GaAs channel, 15 nm GaAs with linearly graded doping $n \rightarrow n^+$ ($n = 2 \times 10^{16} \text{ cm}^{-3}$ and $n^+ = 5 \times 10^{18} \text{ cm}^{-3}$), 8 nm n^+ -GaAs, 2.2 nm AlGaAs, and 50 nm ($\text{Ga}_{0.945}\text{Mn}_{0.055}$)As. Due to the high n^+ -doped GaAs region adjacent to the degenerately p -doped (Ga,Mn)As layer, a tunneling Esaki diode structure is formed at the junction, enabling efficient generation and detection of spin accumulation in n -GaAs. The wafer was patterned into 50 μm wide mesa along [110] direction by standard photolithography and wet chemical etching. Then six ferromagnetic (Ga,Mn)As electrodes (E1 to E6) are defined by electron beam lithography and by wet chemical etching down to the lightly doped n -GaAs channel, as schematically shown in Fig. 1(a) [21–23]. Each ferromagnetic electrode serves a specific purpose; one is

* arakawa@phys.sci.osaka-u.ac.jp

† kensuke@phys.sci.osaka-u.ac.jp

used as an injection electrode (E2), three as detection electrodes (E3, E4, and E5), and two as reference electrodes (E1 and E6). Only the E1 electrode is grounded.

By applying a constant current I_{inj} to E2 (see Fig. 1(a)), we inject spin polarized electrons into the n -GaAs channel. As a consequence, the spin accumulation, i.e., splitting of the chemical potentials ($\Delta\mu = \mu_{\uparrow} - \mu_{\downarrow}$) for up and down spin electrons (μ_{\uparrow} and μ_{\downarrow} , respectively) occurs underneath the injection contact and diffuses to both sides. Figure 1(b) shows a typical spin accumulation signal obtained by measuring the non-local DC voltage difference between contacts E3 and E6 as a function of in-plane magnetic field B . All the measurements were carried out at 1.6 K in a variable temperature insert. The abrupt voltage changes correspond to magnetization switching of E2 or E3. The voltage change ΔV between the parallel (P) and antiparallel (AP) magnetization configurations, which was 0.30 mV in this case, is proportional to $\Delta\mu$ and is given by $\Delta V = \gamma\Delta\mu/e$ [24, 25]. Here, γ is the spin asymmetry coefficient of the tunneling conductance given by $\gamma = (T_1 - T_2)/(T_1 + T_2)$ with $T_{1(2)}$ being the sum of all the transmission probabilities of the tunneling channels from the nonmagnetic GaAs conduction band states to the majority (minority) spin states in the ferromagnetic (Ga,Mn)As. For our device we extract $\gamma = 0.82 \pm 0.03$ for the small I_{inj} limit [21, 23].

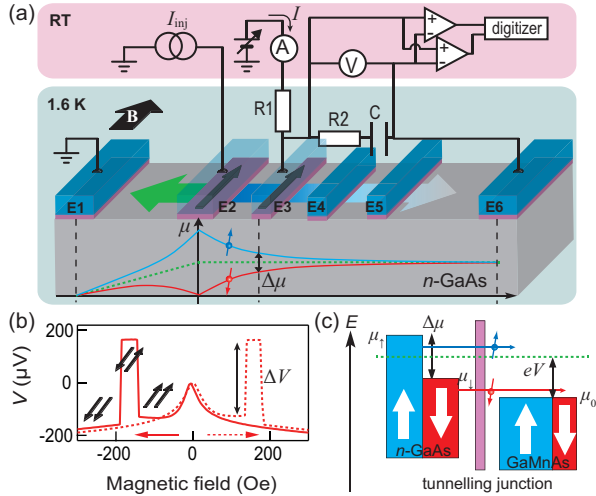


FIG. 1. (color online). (a) Schematic diagram of the sample and measurement system. Six (Ga,Mn)As electrodes (E1 to E6) are placed on the n -GaAs channel, where E2 ($4 \mu\text{m} \times 50 \mu\text{m}$ size) is an injection electrode, while either E3, E4, or E5 ($0.5 \mu\text{m} \times 50 \mu\text{m}$ size) is detection electrode. The center-to-center spacing between the neighboring electrodes is $5 \mu\text{m}$. Schematic spatial dependence of the each chemical potential in the n -GaAs channel is illustrated. (b) Typical non-local voltage signal for $I_{\text{inj}} = -23 \mu\text{A}$. A peak observed around zero magnetic field is induced by dynamic nuclear spin polarization (DNP) [22]. This effect is irrelevant to the present result, as the noise measurement was performed outside of the DNP region. (c) Schematic energy diagram at the tunneling electrode.

We measure the current fluctuations S_I through the tunneling barrier in the presence of spin accumulation generated underneath the given electrode. To measure S_I , we use an additional circuit as shown in Fig. 1(a). Three passive components are placed at 1.6 K; two surface mount metal-film resistors ($R_1 = 1 \text{ M}\Omega$, $R_2 = 1 \text{ k}\Omega$) and a laminated ceramic capacitor ($C = 1 \mu\text{F}$). S_I is converted to voltage noise by R_2 , while R_1 prevents the current noise from leaking to the voltage source. The two sets of voltage noise signals are independently amplified by two amplifiers (NF LI-75A) at room temperature, and are recorded at a two-channel digitizer. Cross-correlation spectrum was obtained in the frequency range between 16 kHz and 160 kHz (9001 points) [26, 27]. To extract S_I across the tunneling barrier, we carefully calibrated the measurement system and eliminate thermal noises from R_2 and the channel resistance [23]. We experimentally confirmed that the contribution of frequency-dependent noise, such as $1/f$ noise, does not affect shot noise for the parameter range we examined.

The measurement procedure is as follows [23]: together with the constant spin injection current I_{inj} , we inject a small current I to one of the detection electrodes (either E3, E4, or E5) using a constant current technique. We directly measure the resulting current I , the voltage drop V , and S_I across the tunneling barrier. The energy diagram is schematically shown in Fig. 1(c). The bias dependence of these values was measured for both P and AP configurations. As I is set between -300 nA and 300 nA , well below I_{inj} , the influence of bias current on the spin accumulation is negligibly small. The data shown in Fig. 2(a) are obtained for injection currents $I_{\text{inj}} = 0, 9$, and $-23 \mu\text{A}$, where electrode E3 is used as detector. Below we discuss the behavior of S_I as a function of V and show that the results match closely the prediction of the Landauer-Büttiker model. For $I_{\text{inj}} = 0 \mu\text{A}$, the observed S_I is independent of the magnetization configuration, and monotonically increases as $|V|$ increases, as expected from conventional shot noise theory [12]. The finite S_I at $V = 0$ is the thermal noise contribution. This curve is perfectly reproduced by the conventional formula given by

$$S_I = \frac{4k_B T_e}{R_d} + 2F \left(eI \coth \left(\frac{eV}{2k_B T_e} \right) - \frac{4k_B T_e}{R_d} \right), \quad (1)$$

where R_d , T_e , and F are the differential resistance at given bias, the electron temperature, and the Fano factor, respectively. For $T_e = 1.6 \text{ K}$, the fitting to this formula gives $F = 0.78 \pm 0.04$ as shown in Fig. 2(a) by the dotted curve. The Fano factor is slightly reduced from unity that is expected for a tunneling junction. This is most probably due to the contribution of defects in the tunneling barrier which are unavoidably created during the (low-temperature) growth process [28–30].

Now, when I_{inj} is finite, i.e. for -9 and $-23 \mu\text{A}$, S_I starts to depend on the magnetization configuration as shown in Fig. 2(a). For example, when $I_{\text{inj}} = -23 \mu\text{A}$, the curves for P and AP behave as if they were hor-

horizontally shifted by 0.28 mV. This voltage shift is in very good agreement with the spin accumulation signal $\Delta V = 0.30$ mV (Fig. 1(b)). This agreement indicates that the present “noise spectroscopy” successfully detects the nonequilibrium chemical potential splitting $\Delta\mu$ due to the spin accumulation (see also Fig. 1(c)) [9]. We emphasize that the observed difference between the two different magnetic configurations is reproducible. Actually, the B -dependence of S_I was measured for constant $V = -6.8$ mV in independent measurements as shown in Fig. 2(b). Clear spin-valve-like changes were observed for $I_{\text{inj}} = -9$ μA and -23 μA reflecting magnetization switching in the electrodes, while no detectable change was observed for $I_{\text{inj}} = 0$ μA . Thus, the configuration-dependent contribution of the noise measured at finite I_{inj} is undoubtedly the shot noise associated with spin accumulation.

In order to distinguish the charge- and spin-associated contributions in the measured current and noise, we adopt the following model based on the Landauer-Büttiker formalism [12, 31]. Currents for P (I_P) and AP

(I_{AP}) states are written as

$$I_P = \frac{e}{h} T_1 (\mu_{\uparrow} - \mu_0) + \frac{e}{h} T_2 (\mu_{\downarrow} - \mu_0), \quad (2)$$

$$I_{AP} = \frac{e}{h} T_2 (\mu_{\uparrow} - \mu_0) + \frac{e}{h} T_1 (\mu_{\downarrow} - \mu_0), \quad (3)$$

where μ_0 is the chemical potential of the (Ga,Mn)As detection electrode (see Fig. 1(c)). The first and second terms in Eqn. (2) and (3) represent tunneling currents with up- and down-spin, respectively. By defining the ratio of transmission probabilities, $\alpha \equiv T_1/(T_1 + T_2)$ and $\beta \equiv T_2/(T_1 + T_2)$, Eqns. (2) and (3) can be rewritten as $I_P = 2(\alpha i_{\uparrow} + \beta i_{\downarrow})$ and $I_{AP} = 2(\beta i_{\uparrow} + \alpha i_{\downarrow})$. Here, $i_{\sigma} = \frac{e}{h} \frac{T_1 + T_2}{2} (\mu_{\sigma} - \mu_0)$ with $\sigma = \uparrow$ or \downarrow are the spin-resolved currents through a hypothetical conductor which has the transmission probability of $\bar{T} (\equiv (T_1 + T_2)/2)$, and is voltage-biased by $(\mu_{\sigma} - \mu_0)/e$. Now, for this conductor, we define the charge current $I_C \equiv i_{\uparrow} + i_{\downarrow} = 2\frac{e}{h}\bar{T} \left(\frac{\mu_{\uparrow} + \mu_{\downarrow}}{2} - \mu_0 \right)$ and spin current $I_S \equiv i_{\uparrow} - i_{\downarrow} = \frac{e}{h}\bar{T} (\mu_{\uparrow} - \mu_{\downarrow})$. Note that conventional (charge) shot noise is driven by the voltage bias, while spin shot noise is driven by the difference of the chemical potentials ($\Delta\mu = \mu_{\uparrow} - \mu_{\downarrow}$), i.e., the spin current driven purely by spin accumulation that would exist in the absence of the ferromagnetic electrode. They can be accessed experimentally by the relations, $I_C = \frac{I_P + I_{AP}}{2}$ and $I_S = \frac{I_P - I_{AP}}{2(\alpha - \beta)}$. By using the experimentally obtained value of γ , we determined α and β as 0.91 and 0.09, respectively. The energy dependence of these values is negligible in the low bias regime in the present experiment. The above discussion is valid for current noise in the parallel configuration $S_P (\equiv \langle (\delta I_P)^2 \rangle / \Delta\nu)$ and the anti-parallel configuration $S_{AP} (\equiv \langle (\delta I_{AP})^2 \rangle / \Delta\nu)$.

For simplicity, consider the case at zero-temperature and the condition $|eV| > \Delta\mu/2$. Assuming that i_{\uparrow} and i_{\downarrow} are independent, which yields $\langle i_{\uparrow} i_{\downarrow} \rangle = \langle i_{\uparrow} \rangle \langle i_{\downarrow} \rangle$ and $\langle (\delta i_{\sigma})^2 \rangle / \Delta\nu = 2eF \langle i_{\sigma} \rangle$, the charge shot noise S_C and spin shot noise S_S in this hypothetical conductor are given by $S_C \equiv 2eF |\langle I_C \rangle| = 2eF (|\langle i_{\uparrow} \rangle + \langle i_{\downarrow} \rangle|) = \frac{S_P + S_{AP}}{2}$ and $S_S \equiv 2eF |\langle I_S \rangle| = 2eF (|\langle i_{\uparrow} \rangle - \langle i_{\downarrow} \rangle|) = \frac{|S_P - S_{AP}|}{2(\alpha - \beta)}$. Note that, because of $|eV| > \Delta\mu/2$, either $|\langle i_{\uparrow} \rangle|, |\langle i_{\downarrow} \rangle| > 0$ or $|\langle i_{\uparrow} \rangle|, |\langle i_{\downarrow} \rangle| < 0$ holds (see Fig. 1(c)). In this discussion, S_C and S_S have the same Fano factor, which is not the general case as discussed below.

Now we come to the central result of the present work. By tuning I_{inj} and/or by choosing different electrodes for detection (E3, E4, or E5), we can perform noise measurements for different values of spin accumulation and $\langle I_S \rangle$. Therefore, we can experimentally derive the relation between S_S and $\langle I_S \rangle$ exactly as in conventional experiments on charge shot noise. In Fig. 2(c), we show the experimental results of S_S vs $\langle I_S \rangle$ and S_C vs $\langle I_C \rangle$ in the range of $|eV| > \Delta\mu/2$ and $|eV| > 2k_B T$ for several values of the injection current and detection electrodes. Now, conventional shot noise theory tells that the charge shot noise is expressed as $S_C \propto \langle I_C \rangle$ for this condition. In fact, S_C is well fitted by the linear function $S_C = 2eF |\langle I_C \rangle|$ (see

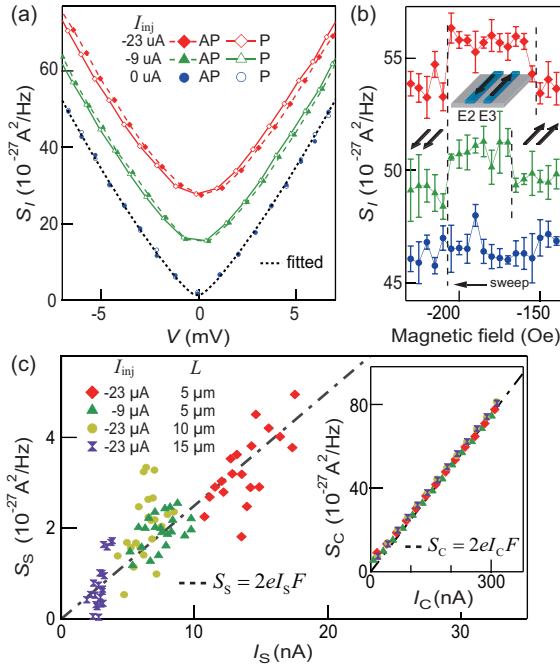


FIG. 2. (color online). (a) Measured S_I at E3 as a function of V for P and AP configurations for several injection currents. The curves are offset vertically by $1 \times 10^{-26} \text{ A}^2/\text{Hz}$ for clarity. The dotted curve is the fitted curve from Eqn. (1). The error bar for each point is $\pm 0.4 \times 10^{-27} \text{ A}^2/\text{Hz}$. (b) B -dependence of S_I measured with keeping V constant ($V = -6.8$ mV) for $I_{\text{inj}} = 0, -9$, and -23 μA (from bottom to top). The thick arrows denote the magnetization directions of E2 and E3. (c) S_S versus I_S for the bias region ($|eV| > \Delta\mu/2, 2k_B T$) for several injection currents and for different detection electrodes. The dashed line is the linear relation with $F = 0.77$. The inset shows the counterpart of the main graph for S_C versus I_C .

inset in Fig. 2(c)), which yields $F = 0.77 \pm 0.04$, consistent with the zero-injection case discussed above (see Fig. 2(a)). Similarly, we find that the spin shot noise S_S also linearly depends on $\langle I_S \rangle$ and, more importantly, satisfies the relation $S_S = 2eF|\langle I_S \rangle|$ (dashed line) with the same Fano factor obtained for the charge shot noise. The coincidence of two Fano factors is the direct consequence of the fact that charge and spin travel through the tunneling barrier as a single entity.

As we mentioned in the beginning, the spin shot noise is expected to occur even without the net charge current as long as the spin current is finite. In this bias region, the shot noise has a unique structure exclusively due to spin shot noise. This is illustrated in Figs. 3(a) and 3(b), which show the results of the simulation based on the above model at zero-temperature [9]. When a non-magnetic material is used for the detection electrode ($\gamma = 0$), a plateau structure appears around zero bias. In contrast, in the case of ferromagnetic electrode (we take $\gamma = 0.5$ for simplicity), the effect that depends on the magnetic configurations occurs for the whole range of the bias voltage. By considering the thermal smearing of the spin-dependent chemical potentials, we can quantitatively explain the present experimental results.

We now estimate the degree of nonequilibrium in terms of the effective electron temperature by fitting $(S_P + S_{AP})/2$ to Eqn. (1). The estimated value of $k_B T_e$ is larger than $\Delta\mu$, indicating that thermal smearing is dominant in the low bias region ($|eV| < 2k_B T_e$). $k_B \Delta T_e$ and $\Delta\mu$ are plotted against I_{inj} and the injector-detector separation L in Figs. 3(c) and 3(d), respectively, where $\Delta T_e (\equiv T_e - 1.6 \text{ K})$ is the effective temperature rise. As

seen in Fig. 3(c), as $\Delta\mu$ increases as a function of I_{inj} , $k_B \Delta T_e$ similarly increases. To the best of our knowledge, direct information such as $k_B \Delta T_e$ to characterize the degree of nonequilibrium due to spin accumulation has never been demonstrated so far. Moreover, as $\Delta\mu$ relaxes according to the diffusion equation, $k_B \Delta T_e$ also relaxes. By fitting $\Delta\mu$ and $k_B \Delta T_e$ to $\Delta\mu \propto \exp(-L/\lambda_S)$ and $k_B \Delta T_e \propto \exp(-L/\lambda_e)$, we obtain spin relaxation length $\lambda_S = 5.6 \mu\text{m}$ and energy relaxation length $\lambda_e = 4.3 \mu\text{m}$ in the channel, respectively (see the dashed curves in Fig. 3(d)). The good agreement between two relaxation lengths indicates that spin relaxation is accompanied by energy relaxation.

Finally, the single-particle picture, we used here, works well since S_C and S_S can be described by using the same Fano factor. In general, however, in the presence of electron-electron interaction and/or spin flips, such a single particle picture is not applicable and the Fano factor would be different for charge and spin shot noise. The spin shot noise physics presented here has significant implications. For example, spin shot noise will be an essentially new probe to explore the spin-transfer torque physics [8], the spin heat accumulation [32], and the spin-dependent chiral edge states in topological insulators [33].

In summary, we have successfully detected the noise associated with the spin current through a tunneling barrier. We defined the charge and spin currents and the charge and spin noises, and proved that the detected spin shot noise demonstrates that charge and spin tunnel through the barrier as a single entity, reflecting both the discrete nature of spin and the spin coherence preservation. As the reality of the fractional charge in fractional quantum Hall states have been proved by shot noise [34, 35], our demonstration of spin shot noise can be the evidence for the reality of spin current.

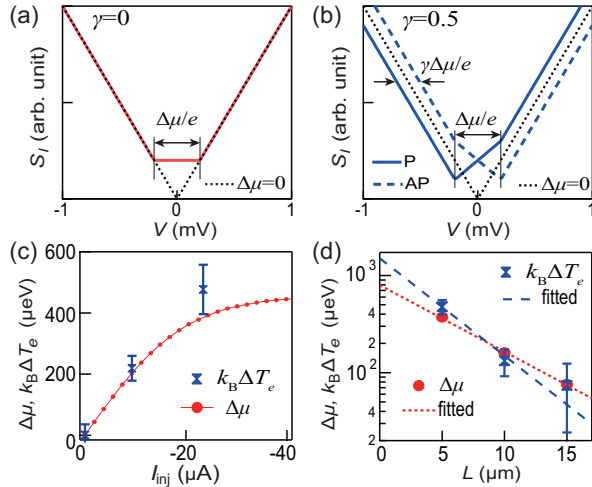


FIG. 3. (color online). (a) and (b) Simulated noise signals at zero-temperature for $\Delta\mu = 400 \mu\text{eV}$, when a non-magnetic ($\gamma = 0$) and a ferromagnetic ($\gamma = 0.5$) detection electrode are used, respectively [9]. The dotted curve indicates shot noise without spin accumulation. (c) I_{inj} -dependence of the extracted $k_B \Delta T_e$ and $\Delta\mu$ at detector E3. (d) L -dependence of $k_B \Delta T_e$ and $\Delta\mu$ for $I_{inj} = -23 \mu\text{A}$.

ACKNOWLEDGMENTS

We appreciate fruitful comments and supports from M. Ferrier and R. Sakano.

-
- [1] W. Schottky, Ann. Phys. (Leipz.) **57**, 541 (1918).
- [2] E. G. Mishchenko, Phys. Rev. B **68**, 100409 (2003).
- [3] W. Belzig and M. Zareyan, Phys. Rev. B **69**, 140407R (2004).
- [4] A. Lamacraft, Phys. Rev. B **69**, 081301(R) (2004).
- [5] B. Wang, J. Wang, and H. Guo, Phys. Rev. B **69**, 153301 (2004).
- [6] J. Foros, A. Brataas, Y. Tserkovnyak, and G. E. W. Bauer, Phys. Rev. Lett. **95**, 016601 (2005).
- [7] A. L. Chudnovskiy, J. Swiebodzinski, and A. Kamenev, Phys. Rev. Lett. **101**, 066601 (2008).
- [8] R. L. Dragomirova, L. P. Žárbo, and B. K. Nikolić, Europhys. Lett. **84**, 37004 (2008).
- [9] J. Meair, P. Stano, and P. Jacquod, Phys. Rev. B **84**, 073302 (2011).
- [10] I. Žutić, J. Fabian, and S. Das Sarma, Rev. of Mod. Phys. **76**, 323 (2004).
- [11] S. M. Sze, K. K. Ng, Physics of Semiconductor Devices. (John Wiley Sons, 2007).
- [12] Ya. M. Blanter and M. Büttiker, Phys. Rep. **336**, 1 (2000).
- [13] Quantum Noise in Mesoscopic Physics, edited by Y. V. Nazarov (Kluwer, Dordrecht, 2003).
- [14] C. W. J. Beenakker and C. Schönenberger, Phys. Today **56**, 37 (2003).
- [15] S. A. Crooker, D. G. Rickel, A. V. Balatsky, and D. L. Smith, Nature **431**, 49 (2004).
- [16] M. Oestreich, M. Romer, R. J. Haug, and D. Hagele, Phys. Rev. Lett. **95**, 216603 (2005).
- [17] S. A. Crooker, J. Brandt, C. Sandfort, A. Greulich, D. R. Yakovlev, D. Reuter, A. D. Wieck, and M. Bayer, Phys. Rev. Lett. **104**, 036601 (2010).
- [18] A. V. Kuhlmann, J. Houel, A. Ludwig, L. Greuter, D. Reuter, A. D. Wieck, M. Poggio, and R. J. Warburton, Nat. Phys. **9**, 570 (2013).
- [19] F. J. Jedema, A. T. Filip, and B. J. van Wees, Nature (London) **410**, 345 (2001).
- [20] X. Lou, C. Adelmann, S. A. Crooker, E. S. Garlid, J. Zhang, K. S. Madhukar Reddy, S. D. Flexner, C. J. Palmstrøm, and P. A. Crowell, Nat. Phys. **3**, 197 (2007).
- [21] M. Ciorga, A. Einwanger, U. Wurstbauer, D. Schuh, W. Wegscheider, and D. Weiss, Phys. Rev. B **79**, 165321 (2009).
- [22] J. Shiogai, M. Ciorga, M. Utz, D. Schuh, T. Arakawa, M. Kohda, K. Kobayashi, T. Ono, W. Wegscheider, D. Weiss, and J. Nitta, Appl. Phys. Lett. **101**, 212402 (2012).
- [23] See Supplemental Material at ** for additional data and discussion.
- [24] A. Fert and H. Jaffrès, Phys. Rev. B **64**, 184420 (2001).
- [25] S. Takahashi and S. Maekawa, Phys. Rev. B **67**, 052409 (2003).
- [26] A. Kumar, L. Saminadayar, D. C. Glatli, Y. Jin, and B. Etienne, Phys. Rev. Lett. **76**, 2778 (1996).
- [27] T. Arakawa, K. Sekiguchi, S. Nakamura, K. Chida, Y. Nishihara, D. Chiba, K. Kobayashi, A. Fukushima, S. Yuasa, and T. Ono, Appl. Phys. Lett. **98**, 202103 (2011).
- [28] R. M. Feenstra, J. M. Woodall, and G. D. Pettit, Phys. Rev. Lett. **71**, 1176 (1993).
- [29] T. Tsuruoka, N. Tachikawa, S. Ushioda, F. Matsukura, K. Takamura, and H. Ohno, Appl. Phys. Lett. **81**, 2800 (2002).
- [30] A. Richardella, P. Roushan, S. Mack, B. Zhou, D. A. Huse, D. D. Awschalom, and A. Yazdani, Science **327**, 665 (2010).
- [31] S. Datta, Electronic Transport in Mesoscopic Systems. (Cambridge Univ. Press, 1997).
- [32] F. K. Dejene, J. Flipse, G. E. W. Bauer, and B. J. van Wees, Nat. Phys. **9**, 636 (2013).
- [33] M. Z. Hasan and C. L. Kane, Rev. of Mod. Phys. **82**, 3045 (2010).
- [34] R. de-Picciotto, M. Reznikov, M. Heiblum, V. Umansky, G. Bunin, and D. Mahalu, Nature **389**, 162 (1997).
- [35] L. Saminadayar, D. C. Glatli, Y. Jin, and B. Etienne, Phys. Rev. Lett. **79**, 2526 (1997).

Supplemental Material

I. ESTIMATION OF THE SPIN ASYMMETRY COEFFICIENT

Here, we explain how to estimate the spin asymmetry coefficient γ_{det} at the detection electrode. The non-local spin-valve signal ΔV as a function of the channel length is described as [24, 25]

$$\Delta V = \frac{\gamma_{\text{inj}}\gamma_{\text{det}}I_{\text{inj}}\lambda_s\rho}{A} \exp\left(-\frac{L}{\lambda_s}\right),$$

where ρ and A are the resistivity and the cross-sectional area of the n -GaAs channel, respectively, and γ_{inj} is the spin asymmetry coefficient at the injection electrode. λ_s and L are, respectively, spin relaxation length and the injector-detector separation as in the main text. In our device, $\rho = 6.7 \times 10^{-4} \Omega\text{m}$ and $A = 50 \text{ m}^2$. By using these values and the estimated λ_s value (see main text), we obtain $\gamma_{\text{inj}}\gamma_{\text{det}}$. Figure 4 shows the obtained $(\gamma_{\text{inj}}\gamma_{\text{det}})^{1/2}$ at E3 as a function of I_{inj} . The value of $(\gamma_{\text{inj}}\gamma_{\text{det}})^{1/2}$ monotonically increases as I_{inj} decreases and saturates at very low bias region, fully consistent with the previous work [22]. Assuming $\gamma = \gamma_{\text{det}} = \gamma_{\text{inj}}$ for sufficiently low bias [21, 22], we obtain $\gamma_{\text{det}} = 0.82 \pm 0.03$, which we use in the main text. Note that I_C in Fig. 3c of the main text is well below $1 \mu\text{A}$ and therefore γ_{det} is constant.

II. DIFFERENTIAL RESISTANCE AT THE DETECTION BARRIER

Here we discuss the differential resistance dV/dI of the tunneling barrier when a spin accumulation is present. Our tunneling junction shows a zero bias peak in dV/dI , which becomes prominent as the temperature lowers. Figure 5 presents the measured dV/dI at the electrode E3 for $I_{\text{inj}} = 0, -9$, and $-23 \mu\text{A}$. For $I_{\text{inj}} = 0$, the peak position is independent of the magnetic configuration, while

for finite I_{inj} the peak positions for P and AP configurations shift to the opposite directions. These shifts are in quantitative agreement with those of the noise signal that are discussed in the main text. Moreover, the peak gets broader as I_{inj} increases. This suggests an increasing electron temperature and is consistent with the behavior of the noise. In the main text, we quantitatively discuss this observation in terms of the effective temperature rise ΔT_e .

III. THE RESULT FOR POSITIVE INJECTION CURRENT

In the main text, we present results only for negative injection currents. Here we present the results for a positive injection current, where the bias direction corresponds to forward biasing of the Esaki diode. Figure 6 shows the measured noise at E3 for $I_{\text{inj}} = 23 \mu\text{A}$. The direction of the horizontal shift of the curves for P and AP alignment is opposite to that found in case of a negative injection current. This is consistent with the reversal of the accumulated spin species. We note that the obtained S_S is proportional to I_S , being consistent with the discussion in the main text.

IV. DETAILS OF NOISE MEASUREMENT AND THE CALIBRATION

Figure 7A shows the detailed set-up of our experiment system. The DC bias voltage of the detection electrode is measured by the multimeter (Keithley 2000) after amplification to avoid noise from the voltmeter. A typical procedure of a noise measurement including magnetization is described as follows:

1. A constant spin injection current I_{inj} is applied to injector E2.

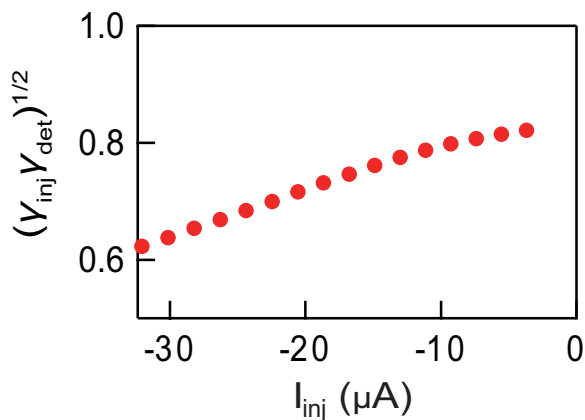


FIG. 4. Spin asymmetry coefficient. The obtained $(\gamma_{\text{inj}}\gamma_{\text{det}})^{1/2}$ at detector E3 as a function of injection current I_{inj} .

2. To saturate the magnetization of injection and detection electrodes, we set $B = 2000 \text{ Oe}$.
3. Then, we set $B = -100 \text{ Oe}$ and measure the bias dependence of the noise for P configuration, where the cross-correlated voltage spectra, the differential resistance, the bias voltage, and the bias current are recorded for each point (see Fig. 7B).
4. To carry out the measurement for AP configuration, we set $B = -175 \text{ Oe}$ and switch the magnetic configuration, and then we set $B = -100 \text{ Oe}$ to measure (see Fig. 7B).

Figure 8 shows the equivalent circuit of the detection line for the DC signal. To measure the current-voltage ($I - V$) characteristic across the detection contact (E3, E4, or E5), we used the constant current method; The bias voltage V_{applied} was applied to the detection contact, whose resistance is typically $45 \text{ k}\Omega$, through the large resistor R1. We directly measured both the current I and the voltage drop V across the detection contact. The measured $I - V$ traces for P and AP configuration are horizontally shifted exactly by the non-local voltage (due to spin accumulation) as shown in the right hand of Fig. 8. Here, the current difference $I_{\text{P}} - I_{\text{AP}}$ for a given voltage is not the change in charge current but the spin current. And consequently the difference of the corresponding noise signals, shown in Fig. 3a, is due to spin shot noise. In order to obtain sufficient resolution of the noise signal, we averaged 15,000 cross-correlation spectra. The typical time to take one point for the noise signal in Fig. 3a in the main text is about 16 min. For the magnetic field dependence shown in Fig. 3b, only 9,000 spectra were averaged, thus the noise signals are slightly scattered when compared to the data in Fig. 3a. The peak around zero magnetic field due to DNP in Fig. 2b and Fig 7B appears within $\pm 100 \text{ Oe}$

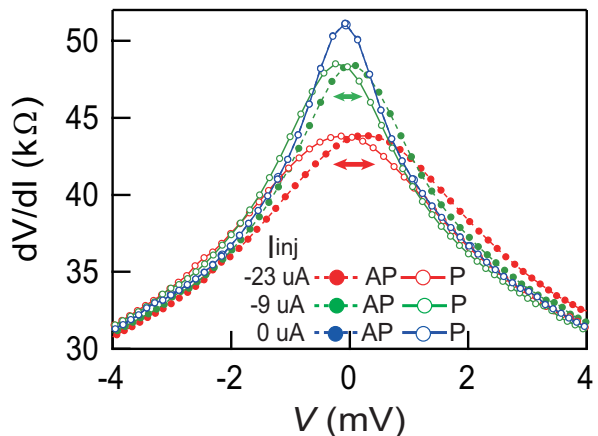


FIG. 5. Differential resistance in the presence of a spin accumulation. Measured dV/dI at detector E3 as a function of V for P and AP configurations for injection currents $I_{\text{inj}} = 0, -9$, and $-23 \mu\text{A}$.

as a Lorentz curve (see the gray dashed curve in Fig. 7B) [22]. Outside the DNP peak, the non-local voltage still decays with increasing external magnetic field but because of a different mechanism. At the measurement temperature, the magnitude of the cubic magnetic anisotropy field of (Ga,Mn)As along [100] and that of the uniaxial anisotropy field along [1-10] are comparable and thus, the total magnetic easy axis lies along somewhere between [100] and [1-10]. When the external magnetic field is swept from zero to either positive or negative direction along the electrode // [1-10], reorientation of the magnetization from the easy axis toward the field occurs. In spin Esaki diodes, the value of the spin asymmetry coefficient of the tunneling conductance λ , i.e., spin injection efficiency, depends on the magnetization orientation with respect to the crystallographic direction of GaAs, which we ascribed to the tunneling anisotropic spin polarization (TASP). Thus, the non-local voltage, a direct measure of spin accumulation, still changes as a function of the magnetic field due to the magnetization reorientation. Moreover, since we averaged for a long time to take each point of the spectrum (typically 16 min for each point), the influence of the DNP is negligibly reduced. To estimate the voltage spectral density S_V , we performed a histogram analysis [27] for the data between 16 kHz and 160 kHz (9,001 points). As mentioned in the method section, the S_V contains not only the intrinsic signal S_I but also extrinsic thermal noise from R2 ($S_I^{R2} = 4k_B T/R2$), the channel resistance R3 ($S_I^{R3} = 4k_B T/R3$), and the input current noise of the amplifier (S_I^{amp}). For example, R3 between the electrodes E3 and E6 is 7.01 k Ω . The contribution of these current noise sources to S_V is given

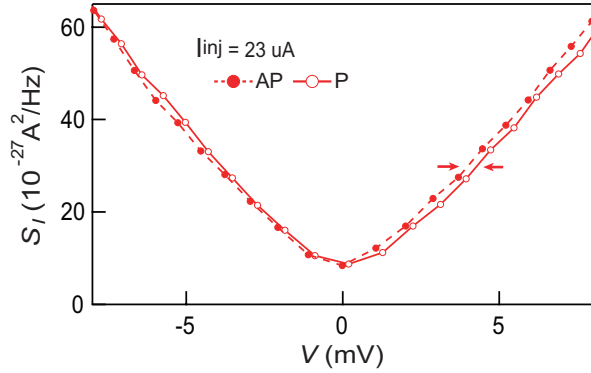


FIG. 6. Measured noise signal for positive injection current and extracted spin shot noise components. Measured S_I at detector E3 as a function of V for P and AP configurations for injection current $I_{inj} = 23 \mu A$.

by

$$\frac{S_V}{G^2} = \left(\frac{\frac{dV}{dT} R2}{\frac{dV}{dT} + R2 + R3} \right)^2 S_I + \left(\frac{\left(\frac{dV}{dT} + R3 \right) R2}{\frac{dV}{dT} + R2 + R3} \right)^2 (S_I^{R2} + S_I^{amp}) + \left(\frac{R2 R3}{\frac{dV}{dT} + R2 + R3} \right)^2 S_I^{R3},$$

where $G = 102.2$ is the gain of the amplifier after cross-correlation is taken into account. In our analysis the S_I^{R2} , S_I^{amp} , and S_I^{R3} contributions are subtracted from the experimentally obtained S_V values by using this equation and the measured stage temperature T .

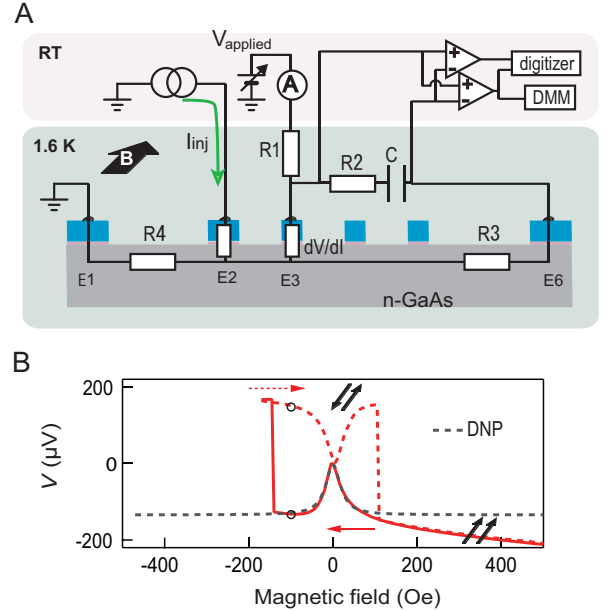


FIG. 7. Schematic illustration of the experiment and a typical spin accumulation signal. A, Schematic diagram of sample and measurement system. dV/dI and R3 are the differential resistance of the detection tunneling barrier and channel resistance between contacts E3 and E6, respectively. B, Non-local voltage signal detected between E3 and E6 as a function of an in-plane magnetic field B for $I_{inj} = -23 \mu A$, where the magnetic field is first ramped from 500 to -175 Oe and then from -175 to 500 Oe. The black circles mark the points where noise measurements were done. The gray dashed curve is a fit of the data with the expected Lorentz curve [22].

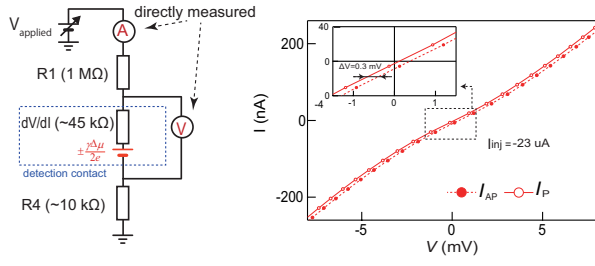


FIG. 8. Schematic circuit used in experiment and a typical $I - V$ curve. An applied voltage V_{applied} drives a constant charge current $I_{\text{P}} + I_{\text{AP}}$. Due to spin-charge coupling a non-local voltage V develops across the ferromagnetic contact E3 (indicated by the modified voltage source) which is measured. This voltage is due to the spin accumulation underneath contact E3 (see Fig. 2c) and drives the spin current $I_{\text{P}} - I_{\text{AP}}$, which can be directly read off from the $I - V$ characteristic, displayed on the right hand side.